Unstable periodic orbits analysis in the Qi system

Lian Jia(贾莲), Chengwei Dong(董成伟)[†], Hantao Li(李瀚涛)[‡], and Xiaohong Sui(眭晓红)

Department of Physics, North University of China, Taiyuan 030051, *China*

(Received 26 September 2022; revised manuscript received 15 November 2022; accepted manuscript online 8 December 2022)

We use the variational method to extract the short periodic orbits of the Qi system within a certain topological length. The chaotic dynamical behaviors of the Qi system with five equilibria are analyzed by the means of phase portraits, Lyapunov exponents, and Poincaré maps. Based on several periodic orbits with different sizes and shapes, they are encoded systematically with two letters or four letters for two different sets of parameters. The periodic orbits outside the attractor with complex topology are discovered by accident. In addition, the bifurcations of cycles and the bifurcations of equilibria in the Qi system are explored by different methods respectively. In this process, the rule of orbital period changing with parameters is also investigated. The calculation and classification method of periodic orbits in this study can be widely used in other similar low-dimensional dissipative systems.

Keywords: chaos, periodic orbits, bifurcation, Qi system

PACS: 05.45.–a, 05.45.Ac, 02.60.Cb **DOI:** 10.1088/1674-1056/aca9c3

1. Introduction

In the late 1880s, Henri Poincaré, in his research on the three-body problem in celestial mechanics, discovered that deterministic systems exhibit aperiodic behavior that is extremely sensitive to initial conditions, which was the first time chaos was detected. In 1963, Lorenz proposed the Lorenz system while studying the atmospheric convection model, which became an important milestone in the history of chaos.[1] In 1999, Chen and Ueta developed a new chaotic attractor called Chen's attractor based on the Lorenz system.[2] In 2002, Lü and Chen proposed a new chaotic system as the transition system between the Lorenz system and the Chen system, which was called the Lü system.[3] Studies of a series of systems including the Lorenz, Chen, Lü and others based on the Lorenz system eventually led to the discovery of the generalized Lorenz-type system.[4–6]

Chaos has become a hot research object in many disciplines and various types of attractors have been proposed.[7–12] In 2005, Qi *et al.* discovered a new three-dimensional (3D) chaotic system with five equilibria, which is special.[13] The significant difference from the Lorenz system is that each equation of the Qi system contains nonlinear terms, and there are many studies on the Qi system. In 2012, the authors studied the adaptive controller and synchronizer of the Qi system,[14] and adaptive control law was designed based on the Lyapunov stability theory to stabilize it to an unstable equilibrium state. Then, global chaos synchronization of identical Qi system with unknown parameters was also designed. The validity of this result was verified by numerical simulation. In Ref. [15], the authors studied the impulsive control and synchronization of the Qi system and some new and less conservative criteria for global exponential stability and asymptotical stability were proposed. The chaotic synchronization of the Qi oscillator with fractional order was investigated in Ref. [16]. The authors proposed suitable conditions for achieving synchronization and the effectiveness of this method was proved by simulation results. In addition, their work proved that advantages of the Qi oscillator in application to secure communication field. The linear and nonlinear generalized synchronization of the Qi system were realized by transmitting only one single variable.[17] In 2017, four forms of energy for the Qi system were uncovered by transforming from the Qi system into the Kolmogorov type system.[18] In Ref. [19], the authors strictly proved the existence of horseshoe in the Qi system. The dimension of the Qi system was reduced by simplifying it into a single integro-differential equation.[20] Recently, there was a conclusion that the dynamics of the Qi system is bi-Hamiltonian.[21] In addition, many four-dimensional hyperchaotic systems were constructed on the basis of the Qi system, and studies showed that they exhibit rich dynamic behaviors and have large hyperchaotic regions.[22–26]

All of the above works do not provide an effective way to classify and study periodic solutions of the Qi system. In the study of long-term behavior of nonlinear systems, due to the sensitive dependence of typical orbits on initial conditions in chaotic motion, it is impossible to predict the physical variable values in detail. Since most conventional methods cannot give accurate results, cycle expansion seems to be a powerful tool for computing dynamical averages, which expresses long-term averaging over chaotic orbits in terms of averages on periodic ones in a hierarchical way.[27,28] The strange attractors of chaotic systems are densely covered by unstable periodic

[†]Corresponding author. E-mail: dongchengwei@tsinghua.org.cn
[‡]Corresponding author. E-mail: lihantao@nuc.edu.cn

© 2023 Chinese Physical Society and IOP Publishing Ltd

orbits. Thus, extracting periodic orbits can help us understand the properties of the strange attractors in the Qi system more deeply. The method of finding unstable periodic orbits has been proposed in the past few decades, and recently the variational method proposed by Lan and Cvitanović can extract unstable periodic orbits more quickly and efficiently.[29] In the practical search for cycles by the variational method, the shorter known periodic orbits can be used as the basic building blocks to construct a longer loop guess by shearing and gluing, which is very effective as the initial guess loop for the calculations of the real periodic orbit. The variational method has been used to calculate cycles in various chaotic systems, which proves its effectiveness.[30–34] For the Qi system, the variational method will continue to play an important role. Since the Qi system is a more complex chaotic system with three nonlinear terms, which implies that its periodic orbits may be more complex. To ensure that all periodic orbits within a certain topological length can be found, symbolic coding is very critical. The coding of periodic orbits based on symbolic dynamics can avoid the occurrence of repeated orbits or the absence of full orbits.[35] For two different parameters of the Qi system, we calculated all short periodic orbits within a certain topological length, and encoded them with two or four letters, respectively. Under one set of the parameters, we unexpectedly found the periodic orbits outside the attractor, which was unprecedented. Besides, compared with Ref. [13], we explored more abundant bifurcation behaviors including local and global bifurcations, demonstrating bifurcations occurrence in different ways.

The rest paper is organized as follows. In Section 2, chaotic dynamic properties of the Qi system are discussed under the parameters $a = 35$, $b = 2.67$, $c = 80$. Section 3 introduces the variational method to extract unstable periodic orbits more effectively. In Section 4, different symbolic encodings under two parameters of the Qi system are investigated, and the periodic orbits outside the attractor are found unexpectedly. Various bifurcations of cycles are explored in Section 5. And two bifurcations of equilibria are explored in Section 6. Finally, Section 7 gives the conclusions.

2. Chaotic dynamics of the Qi system

The Qi system with nonlinear terms in each equation is described by

$$\begin{aligned} \dot{x} &= a(y-x)+yz, \\ \dot{y} &= cx-y-xz, \\ \dot{z} &= xy-bz, \end{aligned} \tag{1}$$

where a, b, and c are the three parameters and yz, xz, xy are three nonlinear terms. Similar to the Lorenz system, the Qi system has symmetry about the z-axis, which is invariant for the coordinate transformation $(x,y,z) \to (-x,-y,z)$. Since there are three cross-product terms, the Qi system has five fixed points, which is relatively rare. These indicate that Qi system has more complex dynamic properties that are worth studying.

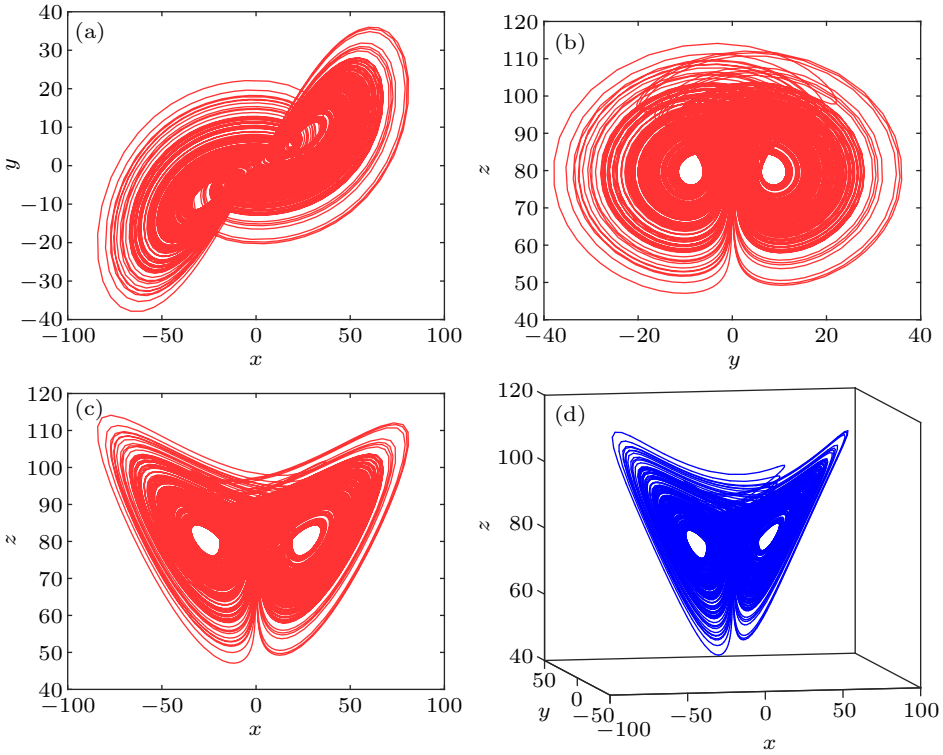


Fig. 1. Phase portraits of the Qi system in different 2D and 3D phase spaces when $a = 35$, $b = 2.67$, $c = 80$.

The equilibria of the Qi system can be obtained by solving the following equations:

$$\begin{aligned} &a(y-x)+yz=0,\\ &cx-y-xz=0,\\ &xy-bz=0. \end{aligned} \tag{2}$$

Under the parameters $a=35$, $b=2.67$, $c=80$, the equilibria of the system are $S_1=(0,0,0)$, $S_2=(26.41,8.06,79.69)$, $S_3=(-26.41,-8.06,79.69)$. S_4 and S_5 are not real equilibria.

Linearization of the Qi system at fixed point S_1 is

$$\boldsymbol{A}=\begin{pmatrix} -35 & 35 & 0\\ 80 & -1 & 0\\ 0 & 0 & -2.67 \end{pmatrix}. \tag{3}$$

According to the Jacobi matrix at S_1, three eigenvalues are obtained: $\lambda_1=-73.5788$, $\lambda_2=37.5788$, $\lambda_3=-2.6700$. Thus, the equilibrium S_1 is a saddle point. Similarly, the Qi system is linearized at the fixed point S_2, and three eigenvalues are obtained according to the Jacobi matrix at S_2: $\lambda_1=-45.9032$, $\lambda_{2,3}=3.6166\pm 32.3640\mathrm{i}$. Since $\lambda_1<0$, the real parts of λ_2 and λ_3 are greater than zero, the fixed point S_2 is a saddle-focus equilibrium. The type of equilibrium S_3 can also be determined by calculating its corresponding Jacobi matrix, which is also a saddle-focus equilibrium. The strange attractor of the Qi system can be seen in Fig. 1.

Periodic orbits can be extracted from the chaotic attractor of the Qi system and the Lyapunov exponents spectrum can help us to confirm the state of the system, as shown in Fig. 2. Under the current parameters, the Lyapunov exponents are: $\lambda_1=4.14696$, $\lambda_2=-0.00281268$, $\lambda_3=-42.8138$, which can also prove that the system is in a chaotic state for the parameters $a=35$, $b=2.67$, $c=80$.

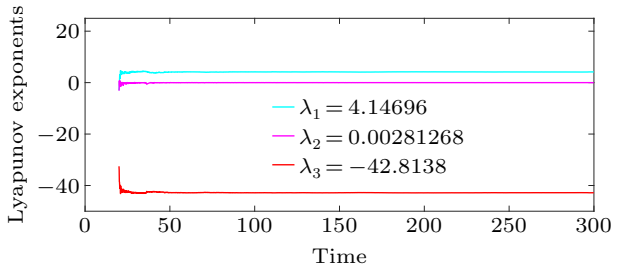


Fig. 2. The Lyapunov exponents spectrum of the Qi system under the parameters $a=35$, $b=2.67$, $c=80$.

The 2D Poincaré section maps, chaotic time series, and consecutive broadband power spectrum of the Qi system can also reflect the chaotic characteristics more comprehensively, as shown in Fig. 3. As the strange attractors of chaotic systems are densely covered by countless unstable periodic orbits, we can have a deeper understanding of the properties of strange attractors of the system by capturing periodic orbits. Therefore, in the next section, we will introduce the method how to calculate the periodic orbits of chaotic systems.

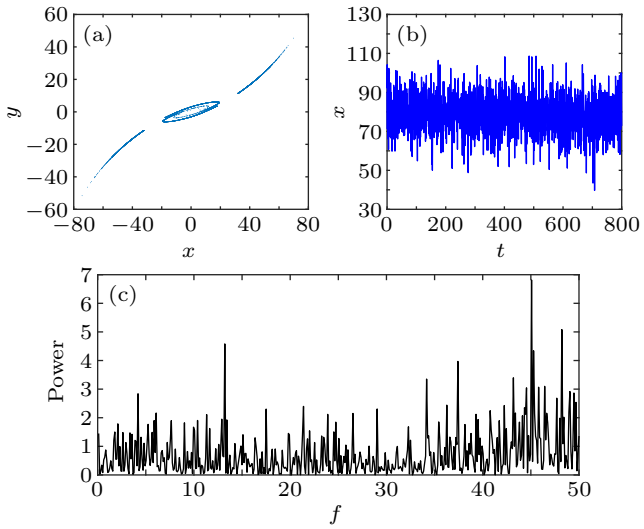


Fig. 3. (a) The 2D Poincaré map on the section $z=79.6948$. (b) Time series for the x signal. (c) The broadband power spectrum.

3. Variational calculation method

Many methods have been proposed to find unstable periodic orbits, such as Newton methods and the multipoint shooting method, which can effectively find unstable periodic orbits in chaotic systems.[36] To find periodic orbits in high-dimensional systems, it is necessary to select multiple Poincaré sections, which is difficult to select in this case. Therefore, Lan and Cvitanović devised the variational method to find unstable periodic orbits, guessing an entire orbit and gradually turning it into a true periodic orbit.[29] This method has good robustness and can quickly converge to the periodic orbit in the process of searching. In the application of the variational method, the following equation is used to describe the evolution of the loop guess $L(\tau)$ to the real periodic orbit p:

$$\frac{\partial^2\widetilde{\boldsymbol{x}}}{\partial s\partial\tau}-\lambda A\frac{\partial\widetilde{\boldsymbol{x}}}{\partial\tau}-\boldsymbol{v}\frac{\partial\lambda}{\partial\tau}=\lambda\boldsymbol{v}-\widetilde{\boldsymbol{v}}, \tag{4}$$

where $\boldsymbol{v}$ represents the flow speed of the system, $\widetilde{\boldsymbol{v}}$ represents the velocity vector of the loop guess which is defined by $\widetilde{\boldsymbol{v}}(\widetilde{\boldsymbol{x}})=\mathrm{d}\widetilde{\boldsymbol{x}}/\mathrm{d}s$, λ is a parameter used to control the period of the cycle, defined by $\lambda(s_n)\equiv\Delta t_n/\Delta s_n$, virtual time τ parametrizes the continuous deformations of the loop. In the process of the evolution of the loop guess to the real cycle, there has a cost function decreasing monotonously

$$F^2[\widetilde{\boldsymbol{x}}]\equiv\frac{1}{2\pi}\oint_{L(\tau)}\mathrm{d}\widetilde{\boldsymbol{x}}\,[\widetilde{\boldsymbol{v}}(\widetilde{\boldsymbol{x}})-\lambda\boldsymbol{v}(\widetilde{\boldsymbol{x}})]^2. \tag{5}$$

In the iterative process, the tangential velocity direction of the loop guess gradually approaches to the flow velocity direction of the system. When they are consistent, the initial loop guess converges to the real periodic orbit as shown in Fig. 4, then the period of the cycle can be calculated by the following equation:

$$T_{\mathrm{p}}=\int_0^{2\pi}\lambda(\widetilde{\boldsymbol{x}}(s,\infty))\,\mathrm{d}s. \tag{6}$$

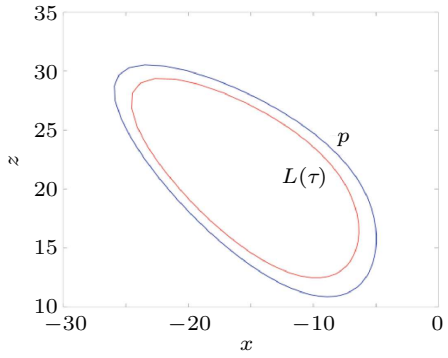


Fig. 4. The evolution of the loop guess $L(\tau)$ into the real periodic orbit p.

In the numerical implementation of the variational calculation method, the finite difference scheme is employed to discretize the loop guess

$$\widetilde{\boldsymbol{v}}_n \equiv \left.\frac{\partial \widetilde{\boldsymbol{x}}}{\partial s}\right|_{\widetilde{\boldsymbol{x}}=\widetilde{\boldsymbol{x}}(s_n)} \approx (\hat{\boldsymbol{D}}\widetilde{\boldsymbol{x}})_n. \tag{7}$$

The five-point approximation is adopted[29]

$$\hat{\boldsymbol{D}} = \frac{1}{12h}\begin{pmatrix} 0 & 8 & -1 & & & & & 1 & -8 \\ -8 & 0 & 8 & -1 & & & & & 1 \\ 1 & -8 & 0 & 8 & -1 & & & & \\ & & & \cdots & & & & & \\ & & & & 1 & -8 & 0 & 8 & -1 \\ -1 & & & & & 1 & -8 & 0 & 8 \\ 8 & -1 & & & & & 1 & -8 & 0 \end{pmatrix}$$

where $h = 2\pi/N$. The discrete version of Eq. (4) is given by

$$\begin{pmatrix} \hat{\boldsymbol{A}} & -\hat{\boldsymbol{v}} \\ \hat{a} & 0 \end{pmatrix}\begin{pmatrix} \delta\widetilde{\boldsymbol{x}} \\ \delta\lambda \end{pmatrix} = \delta\tau\begin{pmatrix} \lambda\hat{\boldsymbol{v}} - \hat{\widetilde{\boldsymbol{v}}} \\ 0 \end{pmatrix}, \tag{8}$$

where $\hat{\boldsymbol{A}} = \hat{\boldsymbol{D}} - \lambda\mathrm{diag}[A_1, A_2, \ldots, A_N]$, $\hat{\boldsymbol{v}} = (\boldsymbol{v}_1, \boldsymbol{v}_2, \ldots, \boldsymbol{v}_N)^{\mathrm{T}}$ and $\hat{\widetilde{\boldsymbol{v}}} = (\widetilde{\boldsymbol{v}}_1, \widetilde{\boldsymbol{v}}_2, \ldots, \widetilde{\boldsymbol{v}}_N)^{\mathrm{T}}$ are the two vector fields that we want to match everywhere along the loop. To solve $\delta\widetilde{\boldsymbol{x}}$ and $\delta\lambda$, the matrix on the left-hand side of Eq. (8) is inverted via the banded LU decomposition on the embedded band diagonal matrix, treating the cyclic and border terms by the Woodbury formula.[37]

In the actual use of the variational method to locate the periodic orbits in the Qi system, we find that initial period conjecture is equally important in the calculations, and it may lead to final non-convergence if there has a little deviation.

4. Periodic orbits of the Qi system

In this section, we use the variational method to extract unstable periodic orbits within a certain topological length of the Qi system for two groups of different parameters. Based on some cycles found, we encode them empirically with two or four letters respectively. We also discover the periodic orbits outside the attractor accidentally. By intuitively observing the periodic orbits extracted from the strange attractor of the Qi system, we can explore the topological properties of periodic orbits in the Qi system more deeply.

4.1. Periodic orbits for $a = 35$, $b = 2.67$, $c = 80$

The parameters are chosen due to the system seems to show interesting chaotic dynamics. We first discuss how to calculate and classify all the short periodic orbits of the Qi system. Symbol sequences can be used to find all periodic orbits within a certain topological length of the Qi system. Topological length refers to the length of symbolic sequence used to represent a cycle. For 1D unimodal maps, there is only one extreme point in the interval, so two symbols can be used to establish the symbolic dynamics of the system.[38] The periodic point on the left is denoted by the symbol 0 and on the right is denoted by the symbol 1. As cycle with an infinite symbol sequence 01010101 is denoted by cycle 01, for the short periodic orbit of length 2, there is only cycle 01. Cycles 000000 and 1111111 are divided into cycles with a topological length of 1, known as cycles 0 and 1. According to this rule, all the periodic orbits can be represented by different symbolic sequences, which can not only distinguish different periodic orbits, but also classify them hierarchically and orderly, to find all short periodic orbits within a certain topological length. By observing the first return map of the Qi system in Fig. 5, we find that it is rather complex and not 1D, with at least four branches, so it is difficult to establish 1D symbolic dynamics to systematically calculate periodic orbits in the usual way. At least four symbols are required to encode the cycles, which brings some difficulties and also means that the dynamic behavior of the Qi system is rich and interesting.

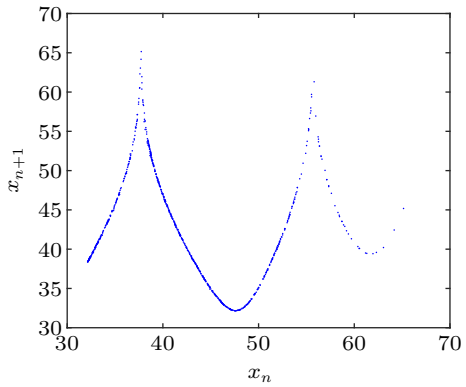


Fig. 5. First return map for Poincaré section $z = 79.6948$.

By studying the found periodic orbits under the current parameters, we find that the cycles have their structures. By comparing the cycles that have been found, we deduce that four short periodic orbits may exist alone or in combination with other orbits. Therefore, these four short periodic orbits can be used as basic building blocks to establish symbolic encodings.

• The smooth cycle that swirls once around the left equilibrium is denoted by the symbol 0, and the smooth cycle that

swirls once around the right equilibrium is denoted by the symbol 1. Cycles 0 and 1 are pruned at the current parameters, and they could only appear in combination with other cycles.

• The smooth cycle in the shape of a raised wing that swirls once around the equilibrium on the left is denoted by the symbol 2, and the smooth cycle in the shape of a raised wing that swirls once around the equilibrium on the right is denoted by the symbol 3.

• All periodic orbits of the Qi system are composed of cycles 0, 1, 2, and 3. Therefore, the longer periodic orbits can also be represented by coding with the above four short periodic orbits as basic building blocks.

Figure 6 shows part of short cycles, which are characterized by distinctive locations and shapes. We classify them according to the above symbolic encodings, and the basic building blocks of the unstable periodic orbits are encoded by cycles 0, 1, 2, and 3. The cycle swirling around the left equilibrium once in Fig. 6(a) is marked as cycle 2. The cycle in Fig. 6(b) is marked as cycle 3. In Fig. 6(c), two elliptical orbit fragments swirl once around the left equilibrium and once around the right, encoded by the symbol 01. The cycle in Fig. 6(d) is marked as cycle 03, which is composed of an elliptical cycle and a cycle with the shape of a raised wing.

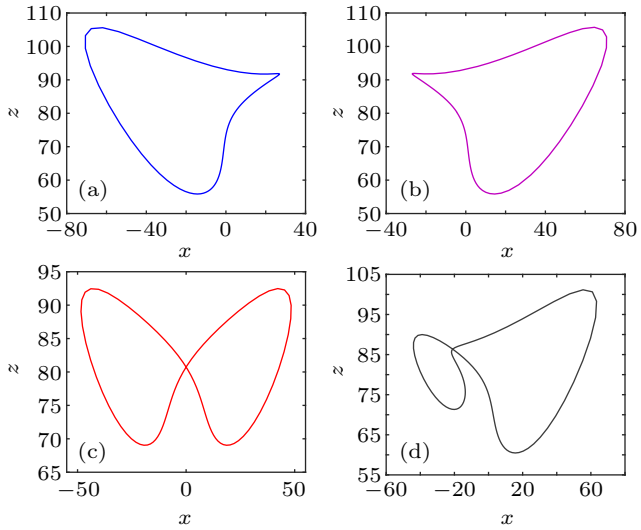


Fig. 6. Short unstable periodic orbits in the Qi system: (a) cycle 2, (b) cycle 3, (c) cycle 01 and (d) cycle 03.

We find 20 unstable periodic orbits with topological length up to 3 by using cycles 0, 1, 2, and 3 as basic building blocks, and the nonexistent periodic orbits are represented by –, as listed in Table 1. As can be seen from Table 1, cycles 001 and 011 have almost equal periods, as are cycles 223 and 233. The above law is determined by the symmetry of the z-axis.

Some of the complex cycles found are shown in Fig. 7. In Fig. 7(a), the elliptical orbital fragments swirl once around the left and right equilibria respectively, and then the orbital fragment in the shape of a raised wing swirls around the left equilibrium once, which is encoded as cycle 012. Figure 7(b) displays cycle 132 that the elliptical orbital fragment firstly swirls around the right equilibrium once, and then the orbital fragments in the shape of a raised wing swirls around the right and left equilibria once respectively. In Fig. 7(c), three orbital fragments in the shape of a raised wing swirl around the left equilibrium twice and the right once, so it is marked as cycle 223. In Fig. 7(d), the elliptical orbital fragments swirl around the right and left equilibria respectively, and then the orbital fragment in the shape of a raised wing swirls around the right equilibrium once, which is named cycle 103, also known as cycle 031. At the same time, it is obvious that it is symmetric with cycle 012 of Fig. 7(a), because of the symmetry of the Qi system about the z-axis.

Table 1. Short periodic orbits up to topological length of 3 in the Qi system for $a = 35$, $b = 2.67$, $c = 80$.

Length	Itineraries	Periods	Itineraries	Periods	Itineraries	Periods
1	0	–	1	–	2	0.337532
	3	0.337532				
2	01	0.424111	02	–	03	0.510122
	12	0.510127	13	–	23	0.663485
3	001	0.644641	002	–	003	0.676139
	011	0.644638	012	0.782167	013	0.739735
	021	0.739728	022	–	023	0.829473
	031	0.782175	032	–	033	0.848801
	112	0.676139	113	–	122	0.848813
	123	–	132	0.829473	133	–
	223	1.002142	233	1.002142		

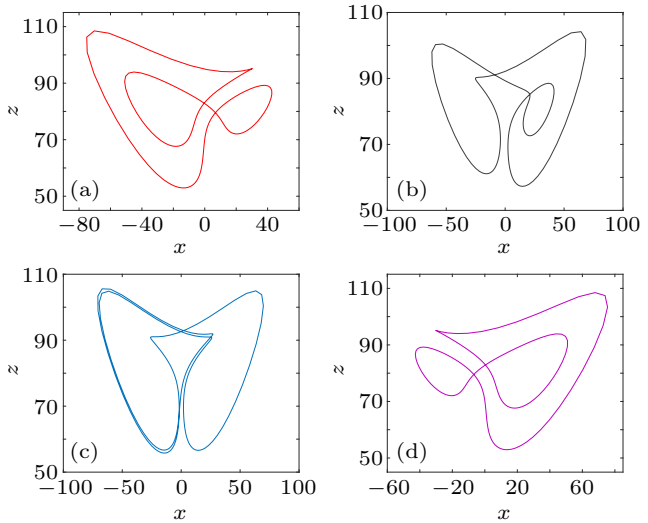


Fig. 7. Four unstable cycles in the Qi system: (a) cycle 012, (b) cycle 132, (c) cycle 223 and (d) cycle 031.

In addition to the above periodic orbits, we also accidentally find another class of short-period orbits with topological length 1. They are the periodic orbits outside the attractor because their self-linking number is 1, which is significantly different from the above orbits. This number represents the linking of a cycle with itself, and for cycle A it can be calculated

as

$$Slk(A) = \sum_i \sigma_i, \tag{9}$$

where σ_i is $+1$ or -1, which represents the signed crossing for the cycle.

As basic building blocks, these orbits can be connected with other periodic orbits. This means that the dynamic characteristics of the Qi system are extremely rich, which is worth exploring. As far as we know, the periodic orbits outside the attractor in the Qi system have not been investigated yet.

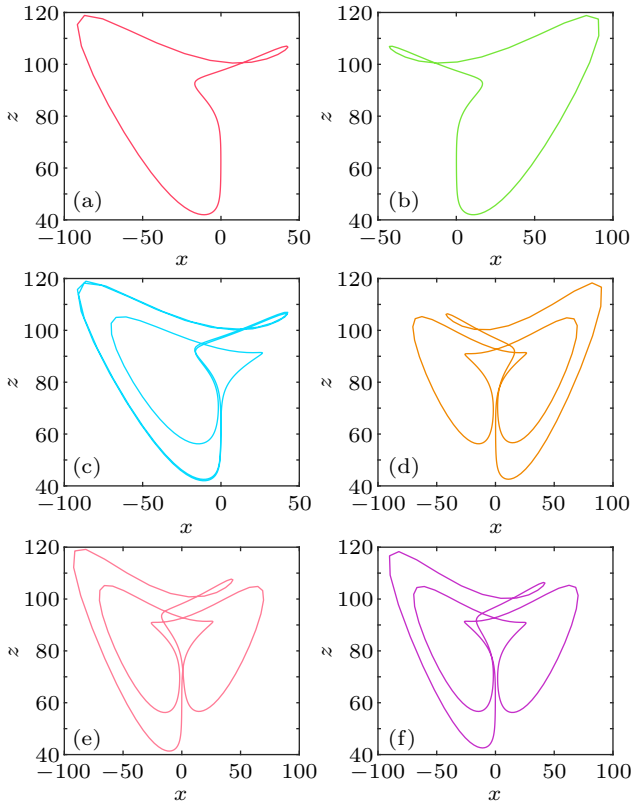


Fig. 8. Six periodic orbits outside the attractor: (a) cycle $2'$, (b) cycle $3'$, (c)cycle $22'2'$, (d) cycle $23'3$, (e) cycle $22'3$, and (f) cycle $32'2$.

Significantly different from cycle 2, the cycle in Fig. 8(a) has a knot in 2D phase space with a self-linking number of 1, which is denoted as cycle $2'$. Similarly, the cycle in Fig. 8(b) is denoted as cycle $3'$. We also show the longer cycles outside the attractor. Figure 8(c) displays cycle $22'2'$ that the orbital fragment in the shape of a raised wing swirls around the left equilibrium, and then two knotted orbital fragments swirl around the left equilibrium. Figure 8(d) displays cycle $23'3$, which consists of two orbital fragments in the shape of a raised wing and one knotted orbital fragment. In Fig. 8(e), the orbital fragments in the shape of a raised wing swirl around the right and left equilibria respectively, and then knotted orbital fragment swirls around the left equilibrium, which is encoded as $22'3$. In Fig. 8(f), the orbital fragments in the shape of a raised wing swirl around the left and right equilibria respectively, and then knotted orbital fragment swirls around the left equilibrium, which is encoded as $232'$, or cycle $32'2$. The symmetric counterpart of cycle $32'2$ is cycle $23'3$. Although the shapes of cycle $32'2$ and cycle $22'3$ are very similar, they are different cycles due to the different order of swirling around the equilibria.

Table 2 lists the periodic orbits outside the attractor we found and their periods. It is not hard to see that the periodic orbits outside the attractor are usually combined with cycle 2 or cycle 3, we speculate that it is probably due to their similar shape. But this is only the empirical law we have summed up. For longer cycles outside the attractor, maybe it can be combined with elliptical cycles, or even all the building blocks 0, 1, 2, 3, $2'$, and $3'$ can be combined at the same time.

Table 2. The periodic orbits outside the attractor in the Qi system for $a = 35$, $b = 2.67$, $c = 80$.

Length	Itineraries	Periods	Itineraries	Periods	Itineraries	Periods
1	$2'$	0.483116	$3'$	0.483116		
2	$2'2$	–	$2'3$	–	$2'3'$	0.966659
3	$22'3$	1.156799	$23'3$	1.143645	$222'$	–
	$232'$	1.143645	$22'2'$	1.295383	$23'2'$	1.295523
	$223'$	1.161324	$233'$	1.156799	$22'3'$	–
	$23'3'$	1.307235	$332'$	1.161324	$32'2'$	1.307235
	$33'2'$	–	$333'$	–	$32'3'$	1.295523
	$33'3'$	1.295383	$2'2'3'$	–	$2'3'3'$	–

4.2. Periodic orbits for $a = 35$, $b = 7$, $c = 22$

It can be seen from the unimodal first return map in Fig. 9 that the Qi system is chaotic under these parameters, so we only need two letters to encode periodic orbits, which has been proved by subsequent calculations. Similarly, only S_1, S_2, and S_3 are real equilibria: $S_1 = (0,0,0)$, $S_2 = (15.5264, 9.6387, 21.3792)$, $S_3 = (-15.5264, -9.6387, 21.3792)$. The Qi system is linearized at the equilibrium S_2, and the eigenvalues are obtained: $\lambda_1 = -42.7676$, $\lambda_{2,3} = -0.1162 \pm 19.7538\mathrm{i}$. Thus, S_2 is a node-focus point. S_3 has the same eigenvalues as S_2, so it is also a node-focus point. The eigenvalues of S_1 are also calculated, which indicates S_1 is a saddle point.

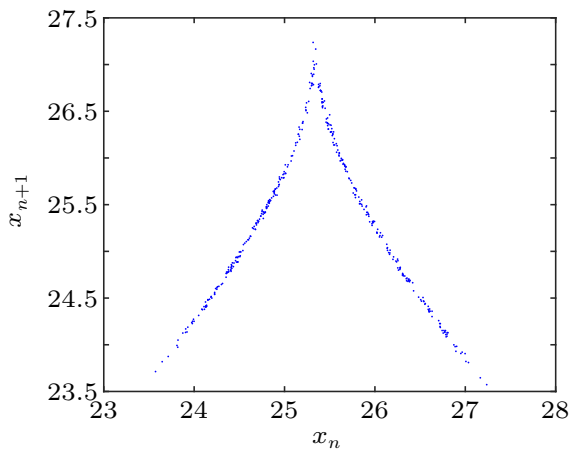


Fig. 9. First return map for the Poincaré section $z = 21.3792$.

Table 3. Short periodic orbits in the Qi syetem for $a = 35,\ b = 7,\ c = 22$.

Length	Itineraries	Periods	Itineraries	Periods	Itineraries	Periods
1	000	0.372581	1	0.372581		
2	01	1.006161				
3	001	1.489072	011	1.489072		
4	0001	1.955562	0011	1.992926	0111	1.955562
5	00001	2.418284	00011	2.470427	00111	2.470426
	01101	2.498620	01111	2.418284	10010	2.498620

The unstable periodic orbits of the Qi system are also calculated. Through the calculation, we find that the periodic orbits under this parameter are relatively simple and all cycles can be encoded with only two letters, which is also verified our conclusion from the first return map. We find all periodic orbits up to topological length of 5 and sort them in Table 3. This shows that the variational method is effective and the classification method based on the topological structure of the orbit is feasible. In some chaotic systems, finding all unstable periodic orbits is a rather difficult task, requiring efficient calculation methods and appropriate symbolic dynamics to ensure that there are no missing orbits. The calculation and classification methods presented here confirm its applicability in the study of low-dimensional dissipative chaotic systems.

5. Bifurcations of cycles in the Qi system

When the parameters of the Qi system change slightly, most of the short periodic orbits will occur the slight deformation. However, the continuous change of parameters may lead to changes in the size and shape of periodic orbits and even stability, which is the bifurcation behavior of the system.[39] To explore the bifurcations in the Qi system, we can use the homotopy evolution method conveniently. Previous periodic orbits with specific parameters can be selected as the initial loop guess with slight parameter changes, so that the initial loop guess with new parameters is closer to the real cycle and smoother. In this way, the number of iterations will be reduced and the computational efficiency will be greatly improved by using homotopy evolution to initialize and search for real periodic orbits.

5.1. The pitchfork bifurcation and period-doubling bifurcation

For the convenience of the study, we choose the short periodic cycles with topological length 2 as the research object. Fixed $a = 35$, $c = 25$, the deformation of symmetric cycle 01 and asymmetric cycles 12 and 03 with the change of b value is studied. We find that symmetric cycle 01 is stable when $b \leq 1.99$. And there is no asymmetric cycle, that is, there are no cycles 03 and 12 when $b \leq 1.99$. When $b > 1.99$, symmetric cycle 01 starts to become unstable, asymmetric cycles 12 and 03 appear. At which point, cycles 12 and 03 are stable. Therefore, we conclude that the pitchfork bifurcation occurs in the Qi system when $b = 1.99$. We also calculate the Lyapunov exponents of the Qi system under the parameters $a = 35,\ b = 1.99,\ c = 25$ in Fig. 10: $\lambda_1 = 0.00834819$, $\lambda_2 = -0.0313277$, and $\lambda_3 = -37.9669$, since the two largest Lyapunov exponents are close to zero, which confirms that the pitchfork bifurcation does occur here.

Keeping the parameters $a = 35$, $c = 25$ unchanged, we also draw the bifurcation diagram versus parameter b in Fig. 11. It can be seen that the pitchfork bifurcation occurs at about $b = 1.99$, and there exists period-doubling bifurcation route to chaos.

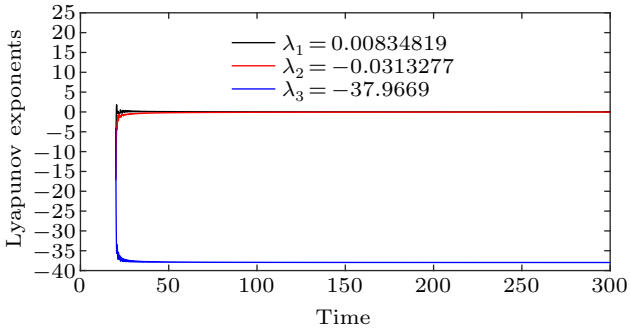


Fig. 10. Lyapunov exponents spectrum of the Qi system when $a = 35$, $b = 1.99$, $c = 25$.

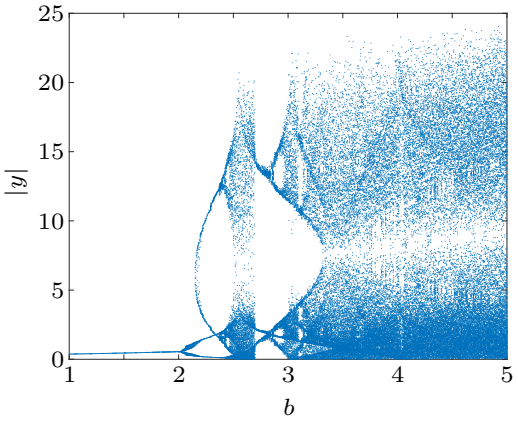


Fig. 11. Bifurcation diagram of the Qi system.

The pitchfork bifurcation and period-doubling bifurcation always occur very close. As the value of b continues to increase, we find that when $b > 2.471$, the asymmetric cycles 03 and 12 begin to become unstable. In order to clearly see the influence of different initial values on the corresponding orbits, we draw the basin of attraction, which is defined as the set of initial conditions under which the orbits converge to a given attractor, as shown in Fig. 12. The yellow and blue regions indicate that these initial values will evolve into unstable orbits 03 and 12, respectively. We deduce that a period-doubling bifurcation occurs at $b = 2.471$. At this point, we also calculate the Lyapunov exponents in Fig. 13, and the two largest Lyapunov exponents are also close to zero. From another point of view, it is proved that a bifurcation occurs.

Table 4. The process and characteristics of the bifurcations.

	Cycle 01	Cycles 03 and 12
$b < 1.99$	stable	non-existence
$b = 1.99$	the pitchfork bifurcation	
$1.99 < b < 2.471$	unstable	stable
$b = 2.471$	the period-doubling bifurcation	
$b > 2.471$	unstable	unstable

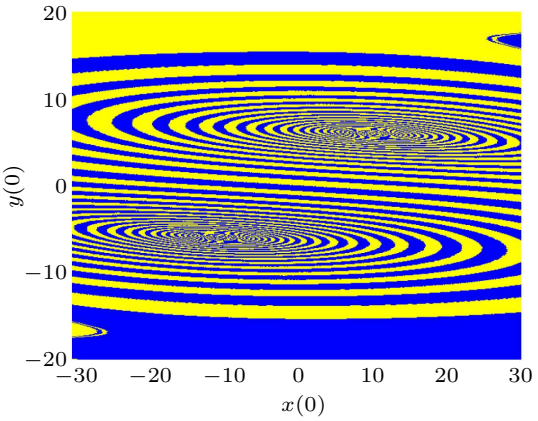


Fig. 12. Basins of attraction in the $x(0)$–$y(0)$ initial plane with $z(0) = 24.41$.

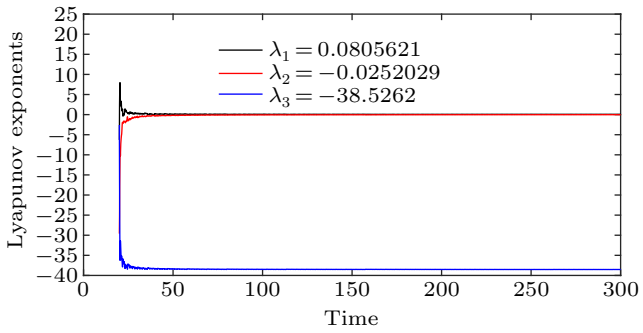


Fig. 13. Lyapunov exponents spectrum of the Qi system when $a = 35$, $b = 2.471$, $c = 25$.

For clarity, the stability of the three cycles, as well as bifurcations that occur at different b values, are shown in Table 4.

To have a more comprehensive understanding of the dynamic characteristics of the Qi system changing with parameters, we also draw a division of parameters in Fig. 14. We choose fixed $c = 25$ to calculate the largest Lyapunov exponents with different parameters a and b. The magnitude of the maximum Lyapunov exponent is related to the colors of the map, which indicate different dynamic behaviors. The parameters are selected as $a \in [25, 50]$, $b \in [0, 20]$. As shown in Fig. 14, near the red area, the largest Lyapunov exponent of the system is greater than 0, indicating that the system is chaotic. The largest Lyapunov exponent in the light green part is close to 0, and the system is periodic. Near the blue region, the largest Lyapunov exponent of the system is less than zero, and the orbits will converge to the fixed point. From the division diagram, we can also see the approximate locations where the pitchfork bifurcation and period-doubling bifurcation occur. It can be seen that the color at the bifurcations is light green, and the corresponding largest Lyapunov exponent is near 0, which is consistent with our homotopy evolution results mentioned above.

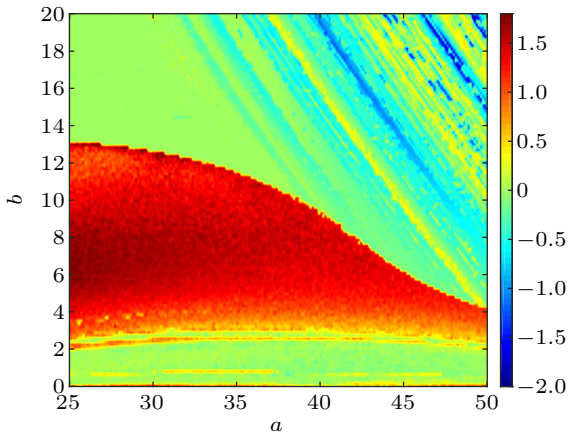


Fig. 14. Division of parameters $a \in [25, 50]$, $b \in [0, 20]$ when $c = 25$.

5.2. The periodic orbit bifurcation and saddle-node bifurcation

We select the fixed parameters $a = 35$, $b = 2.67$ and change the value of c to observe the deformation of cycles 2 and 3, and periods of cycle 2 corresponding to different c values are selected and listed in Table 5. The periods of cycle 3 are consistent with that of cycle 2. We find that the existing cycles 2 and 3 suddenly disappear when $c < 27$, which means that cycles 2 and 3 are pruned within this parameter range, so we conclude that periodic orbit bifurcation occurs at $c = 27$. When $c = 27$, cycles 2 and 3 both exist independently, with completely different shapes. In the process of increasing the value of c, we find that cycle 2 and cycle 3 become more and more similar, eventually collide at $c = 328.735$ and disappear together soon after. Therefore, we have concluded that a saddle-node bifurcation occurs at $c = 328.735$. Figure 15 shows the continuous deformations of cycles 2 and 3 as the c value changes. The characteristics of the cycles during the change of c value are listed in Table 6.

Table 5. The periods of cycle 2 for different c values.

c values	Periods
27	1.141201
50	0.505848
80	0.337525
120	0.245948
160	0.197948
190	0.174006
220	0.155828
240	0.145891
260	0.137258
280	0.129668
300	0.122929
328.735	0.114451

Table 6. The process and characteristics of the bifurcations.

	Cycles 2 and 3
$c < 27$	non-existence
$c = 27$	the periodic orbit bifurcation
$27 < c < 328.735$	independent existence
$c = 328.735$	the saddle-node bifurcation
$c > 328.735$	non-existence

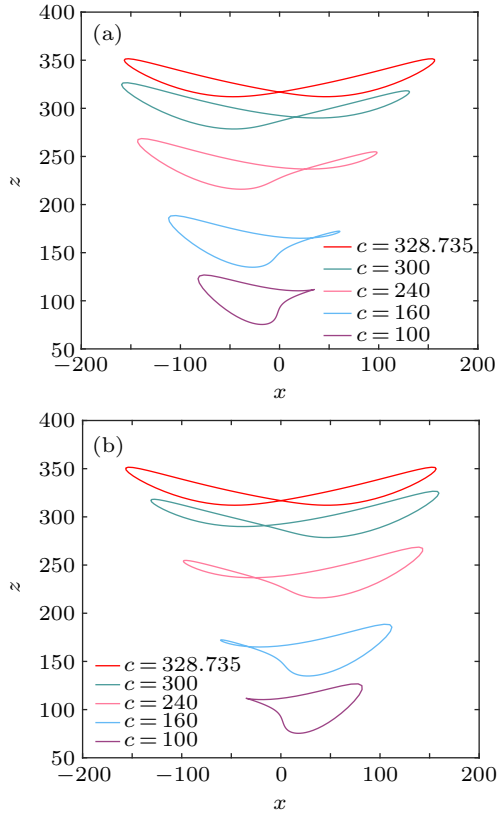


Fig. 15. Continuous deformation of cycles 2 and 3.

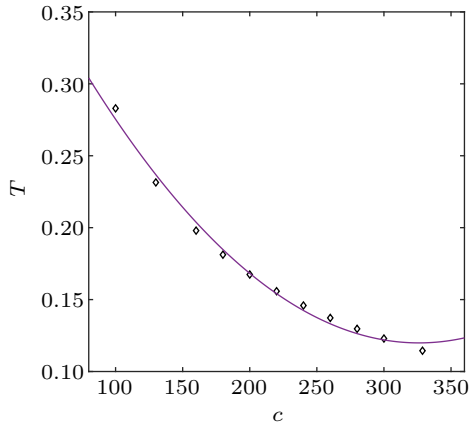


Fig. 16. The periods of cycle 2 for different c values.

We also fit the curve that the periods of cycle 2 vary with the values of c as shown in Fig. 16. The expression of the period of the cycle for the value of c is $T = 3\times10^{-6}c^2 - 0.002c + 0.44$. Based on a certain number of cycles found, we can calculate the orbital period of the next parameter approximately by numerical fitting, which can be used in the variational calculations, to greatly improve the efficiency of searching for real cycles.

6. Bifurcations of equilibria in the Qi system

When the parameters change, the number and stability of equilibria will also change, and this change will also lead to bifurcation. The difference is that the cycles of three-dimensional and above high-dimensional chaotic systems can hardly be obtained by analytical method, while the equilibria can be obtained accurately. Because the bifurcation of cycles is not a point, but a very small neighborhood. The two bifurcations we study next are both bifurcations of equilibria, which are solved mathematically and proved by numerical methods.

6.1. The pitchfork bifurcation

There always has equilibrium $S_1 = (0,0,0)$, the characteristic equation at S_1 is

$$\begin{aligned} P(\lambda) &= \lambda^3 + (a+1+b)\lambda^2 + (a+ab+b-ac)\lambda - abc + ab \\ &= 0, \end{aligned} \tag{10}$$

with the corresponding eigenvalues

$$\lambda_{1,2} = \frac{-(a+1) \pm \sqrt{(a+1)^2 - 4(a-ac)}}{2},$$

$\lambda_3 = -b$. Given $a+1 \neq 0$ and $b \neq 0$, if $a - ac < 0$, equilibrium S_1 is a hyperbolic saddle which has eigenvalues $\lambda_{1,2}$ of real numbers with different signs. The saddle S_1 has a two-dimensional unstable manifold and a one-dimensional stable manifold for $b < 0$, and S_1 has a one-dimensional unstable manifold and a two-dimensional stable manifold for $b > 0$. If $a - ac > 0$ and $\Delta \geq 0$, S_1 is a saddle or node which has eigenvalues $\lambda_{1,2}$ of real numbers with same signs. If $a - ac > 0$ and $\Delta < 0$, S_1 is a saddle-focus or node-focus with a pair of simple complex-conjugate eigenvalues $\lambda_{1,2}$. Therefore, the pitchfork bifurcation occurs at $c = 1$, and the corresponding equilibrium S_1 has one zero eigenvalue and two nonzero real eigenvalues. The following is a detailed proof of the bifurcation.

We construct the following equivalent expression of the Qi system to determine the nature of the stability of equilibrium S_1 for $c = 1$:

$$\begin{aligned} \dot{x} &= a(y-x) + yz, \\ \dot{y} &= x - y + \bar{c}x - xz, \\ \dot{z} &= xy - bz, \end{aligned} \tag{11}$$

where $\bar{c} = c - 1$ is a parameter. Thus, $\bar{c}x$ is a nonlinear term, linearizing at equilibrium S_1

$$\boldsymbol{A}_1 = \begin{pmatrix} -a & a & 0 \\ 1 & -1 & 0 \\ 0 & 0 & -b \end{pmatrix}. \tag{12}$$

The eigenvalues are given: $\lambda_1 = 0$, $\lambda_2 = -a-1$, $\lambda_3 = -b$, with the corresponding eigenvectors

$$\boldsymbol{\xi_1} = \begin{pmatrix} 1 \\ 1 \\ 0 \end{pmatrix}, \quad \boldsymbol{\xi_2} = \begin{pmatrix} 1 \\ -a \\ 0 \end{pmatrix}, \quad \boldsymbol{\xi_3} = \begin{pmatrix} 0 \\ 0 \\ 1 \end{pmatrix}.$$

The system (11) is transformed by using the eigenvectors

$$\begin{pmatrix} \dot{u} \\ \dot{v} \\ \dot{w} \end{pmatrix} = \begin{pmatrix} 0 & 0 & 0 \\ 0 & -a-1 & 0 \\ 0 & 0 & -b \end{pmatrix} \begin{pmatrix} u \\ v \\ w \end{pmatrix}$$

$$+ \begin{pmatrix} (a+1)^{-1}(awu - a^2wv + u\bar{c} - uw + v\bar{c} - vw) \\ (a+1)^{-1}((u-av)w - (u+v)(\bar{c}-w)) \\ (u+v)(u-av) \end{pmatrix}. \quad (13)$$

Therefore, according to the central manifold theory, the Qi system has a two-dimensional central manifold which can be expressed as a function of the variables u and c. The stability of equilibrium S_1 near $\bar{c} = 0$ can be determined by studying first-order ordinary differential equations on the central manifold. The central manifold can be represented as

$$W^{\mathrm{c}}(0) = \left\{ (u,\bar{c},v,w) \in R^4 \middle| v = V(u,\bar{c}),\ w = W(u,\bar{c}),\ V(0,0) = W(0,0) = 0,\ DV(0,0) = DW(0,0) = 0 \right\}. \quad (14)$$

Assuming that

$$\begin{aligned} \dot{V} &= b_1u^2 + b_2u\bar{c} + b_3\bar{c}^2 + O(3), \\ \dot{W} &= c_1u^2 + c_2u\bar{c} + c_3\bar{c}^2 + O(3), \end{aligned} \quad (15)$$

where $O(3)$ expresses the higher-order terms of order equal to or greater than 4. Substituting the expressions of $\dot{V}$ and $\dot{W}$ into Eq. (13), the undetermined coefficients can be obtained as

$$V = -2(a+1)^{-2}u\bar{c} + O(3), \quad W = b^{-1}u^2 + O(3). \quad (16)$$

Substituting expression (16) into Eq. (13), we obtain the restricting vector field of Eq. (13) on its center manifold as follows:

$$\begin{aligned} \dot{u} &= U(u,\bar{c}) \\ &= b^{-1}(a-1)(a+1)^{-1}u^3 + 2b^{-1}(a^2+1)(a+1)^{-3}u^3\bar{c} \\ &\quad + (a+1)^{-1}u\bar{c} - 2(a+1)^{-3}u\bar{c}^2 + O(4), \\ \dot{\bar{c}} &= 0. \end{aligned} \quad (17)$$

Since the higher order terms have little influence on the flow, the cubic differential equation is sufficient to determine the stability of the equilibrium

$$\begin{aligned} F(u,\bar{c}) &= b^{-1}(a-1)(a+1)^{-1}u^3 + 2b^{-1}(a^2+1)(a+1)^{-3}u^3\bar{c} \\ &\quad + (a+1)^{-1}u\bar{c} - 2(a+1)^{-3}u\bar{c}^2. \end{aligned}$$

Since

$$\begin{aligned} &F(0,0) = 0, \quad \left.\frac{\partial F}{\partial u}\right|_{u=0,\bar{c}=0} = 0, \quad \left.\frac{\partial F}{\partial \bar{c}}\right|_{u=0,\bar{c}=0} = 0, \\ &\left.\frac{\partial^2 F}{\partial u^2}\right|_{u=0,\bar{c}=0} = 0, \quad \left.\frac{\partial^2 F}{\partial u \partial \bar{c}}\right|_{u=0,\bar{c}=0} = (a+1)^{-1} \neq 0, \\ &\left.\frac{\partial^3 F}{\partial u^3}\right|_{u=0,\bar{c}=0} = 6b^{-1}(a-1)(a+1)^{-1} \neq 0, \end{aligned}$$

it is proved that the Qi system experiences the pitchfork bifurcation at $c = 1$ according to the correlative pitchfork bifurcation theory.[40]

In the local neighborhood of $c = 1$, when $c < 1$, Qi system has only one stable equilibrium S_1. When $c > 1$, S_1 becomes an unstable equilibrium, and two stable equilibria are generated simultaneously. Let $a = 35$, $b = 2$, $c = 6$, the two non-zero equilibria are $S_2 = (3.429, 2.99, 5.128)$ and $S_3 = (-3.429, -2.99, 5.128)$, and they are symmetric about the z-axis. Selecting two points near the origin as initial values, they will move away from the zero equilibrium and be attracted to the equilibrium point $S_{2,3}$, which indicates that the two non-zero equilibria are stable, as shown in the Fig. 17. Therefore, our conclusion that the pitchfork bifurcation occurs at $c = 1$ is numerically proved.

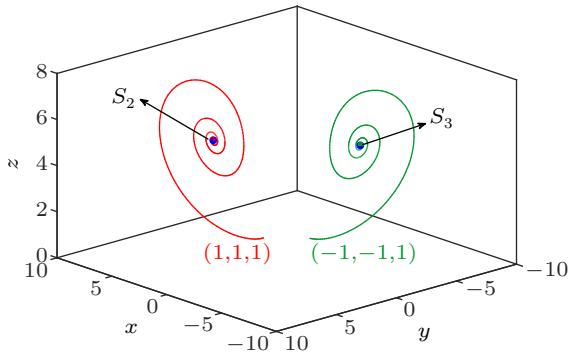


Fig. 17. The 3D phase portrait of the Qi system for $a = 35$, $b = 2$, $c = 6$. Initial conditions $I_2(1,1,1)$ and $I_3(-1,-1,1)$ lead to asymptotically converging behaviors to equilibrium point S_2 and S_3, respectively.

6.2. The Hopf bifurcation

When $b = 1.5$, $c = 25$, it can be known that the Qi system has three equilibria after calculation: $S_1 = (0,0,0)$ and $S_{2,3} = (\pm x_0, \pm y_0, z_0)$, where

$$\begin{aligned} x_0 &= \frac{9}{2a^2}\sqrt{25\sqrt{a^2+46a+625}+23a+625}, \\ y_0 &= \frac{\sqrt{3a\left(25\sqrt{a^2+46a+625}+23a+625\right)}}{\sqrt{a^2+46a+625}+a+25}, \\ z_0 &= \frac{25\sqrt{a^2+46a+625}+23a+625}{\sqrt{a^2+46a+625}+a+25}, \quad a \in R. \end{aligned}$$

The Qi system is invariant for the coordinate transformation $(x,y,z) \to (-x,-y,z)$, so equilibria S_2 and S_3 have the same stability. The Jacobian of the Qi system, evaluated at S_2, is

$$\boldsymbol{A}_2 = \begin{pmatrix} -a & a+z_0 & y_0 \\ 25-z_0 & -1 & -x_0 \\ y_0 & x_0 & -1.5 \end{pmatrix}.$$

The linearized system at the equilibrium S_2 has the characteristic equation

$$\begin{aligned} \det(\lambda \boldsymbol{I} - \boldsymbol{A}) \; = \; & \lambda^3 + (a+2.5)\lambda^2 \\ & + (az - y^2 + x^2 + z^2 - 22.5a - 25z + 1.5)\lambda \\ & + axy + ax^2 + 2xyz + 1.5az \\ & - 25xy + 1.5z^2 - y^2 - 37.5z - 36a. \end{aligned} \tag{18}$$

When parameter a varies and passes through the critical value a_0, the Qi system undergoes a Hopf bifurcation at S_2. The characteristic equation of the Qi system has a pair of pure imaginary roots when $a = a_0$, $\lambda_{1,2} = \pm \mathrm{i}$ and another root λ_3. Substituting it into Eq. (18) yields $\lambda_1 + \lambda_2 + \lambda_3 = -(a+2.5)$, obviously, $\lambda_3 = -(a+2.5)$. Then, by tedious calculations, we conclude that the Hopf bifurcation occurs at $a_0 = 47$. And the eigenvalues of $S_{2,3}$ are computed as $\lambda_1 = -46.5$, $\lambda_{2,3} = \pm 10.2\mathrm{i}$. The first condition for the Hopf bifurcation is met.[41] Differentiating all the terms in Eq. (18) with respect to the parameter a, one obtains

$$\lambda'(a) = \frac{-\lambda^2 - z\lambda + 22.5\lambda - xy - x^2 - 1.5z + 36}{3\lambda^2 + 5\lambda + 2a\lambda - y^2 + x^2 + z^2 - 25z + 1.5 + az - 22.5a}.$$

So $\mathrm{Re}(\lambda'(a_0 = 47))|_{\lambda = 10.2\mathrm{i}} \neq 0$, $\mathrm{Im}(\lambda'(a_0 = 47))|_{\lambda = 10.2\mathrm{i}} \neq 0$. Therefore, the second condition for a Hopf bifurcation is also satisfied.[41] Thus, the Hopf bifurcation exists in the system.

In order to justify the above theoretical analysis on Hopf bifurcation of the Qi system, we will prove the occurrence of the Hopf bifurcation from the numerical point of view. For the parameters $a = 53$, $b = 1.5$, $c = 25$, we can compute the fixed points of the system: $S_{2,3} = (\pm 7.29, \pm 5.00, 24.31)$. The Jacobian eigenvalues at S_2 and S_3 can be obtained as $\lambda_1 = -55.3568$, $\lambda_{2,3} = -0.0716 \pm 10.0432\mathrm{i}$. It can be seen from the eigenvalues that S_2 and S_3 are both stable node-focus points. Under the parameters, we obtain the coexistence of three attractors, as shown in Fig. 18. Orbits starting from initial conditions (17, 11.5, 25.23) and $(-17, -11.5, 25.23)$ spirally converge to S_2 and S_3, respectively. However, the trajectory starting from initial conditions (20.8190, 15.8485, 25.2307) converges to a periodic orbit. To more clearly show the initial point distributions of different attractors, we draw the basin of attraction with the section $z = 24.31$, as shown in Fig. 19. The basins of attraction show that there are three kinds of attractors under this parameter, where yellow and red areas represent that the motion from these initial points will converge to equilibria S_2 and S_3, respectively, and blue areas represent the periodic attractor.

However, when $a < 47$, only the solution of bifurcating periodic attractor exists in the system, as shown in Fig. 20. This means that the subcritical Hopf bifurcation of the Qi system occurs at $S_{2,3}$.

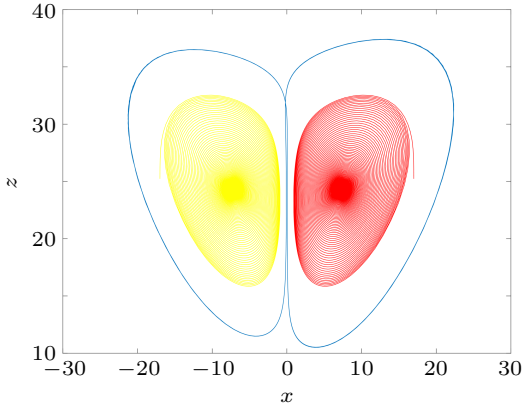


Fig. 18. Three coexisting hidden attractors of the Qi system for $a = 53$, $b = 1.5$, $c = 25$.

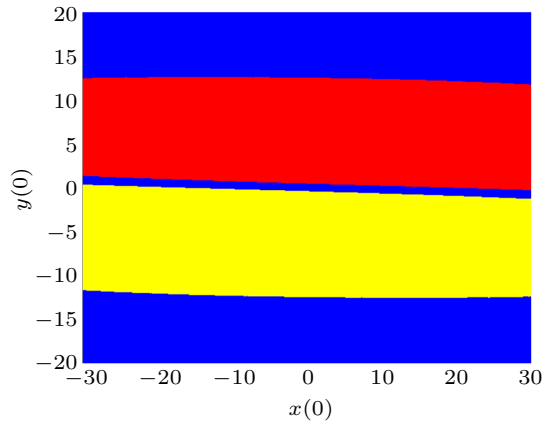


Fig. 19. Basins of attraction for the Qi system at $z = 24.31$. Yellow and red basins represent attractors of two stable node-focus points S_2 and S_3, and blue areas denote the periodic attractor.

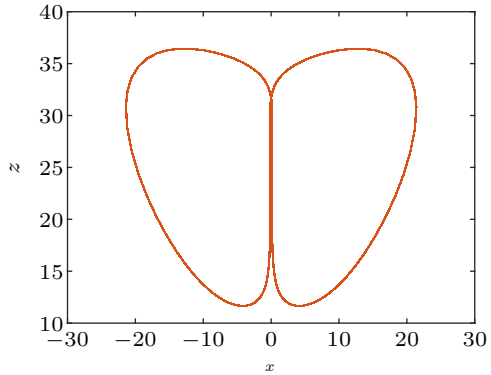


Fig. 20. The periodic attractor of the Qi system for $a = 50$, $b = 1.5$, $c = 25$.

7. Conclusion

Short periodic orbits of the Qi system are calculated via the variational method. Symbolic encodings with two let-

ters and four letters are established respectively based on the trajectory topology with two groups of different parameters, which proves that symbolic encodings are effective for the classification of all short periodic orbits. We also find unstable periodic orbits outside the attractor, which have a more complex topological structure.

In addition, we study the bifurcations of cycles and the bifurcations of equilibria by different methods. For bifurcations of cycles, we use the homotopy evolution approach to analyze the continuous deformation of different cycles, so as to determine the location of the bifurcation, and prove the occurrence of bifurcations under specific parameters by Lyapunov exponents, bifurcation diagram, basins of attraction, division of parameters and other methods. We also discuss the evolution rule of the orbital period with parameters changed. In a certain range, the period of cycle 2 decreases with the increase of c. For the bifurcations of equilibria, we use the analytical method to calculate the bifurcations, and put the specific value to prove the occurrence of bifurcations by numerical way. This work will provide some reference for the search of unstable periodic orbits for other chaotic systems.

Acknowledgments

Project supported by the National Natural Science Foundation of China (Grant Nos. 12205257, 11647085, and 11647086), the Shanxi Province Science Foundation for Youths (Grant No. 201901D211252), Fundamental Research Program of Shanxi Province (Grant No. 202203021221095), and the Scientific and Technological Innovation Programs of Higher Education Institutions in Shanxi of China (Grant Nos. 2019L0505, 2019L0554, and 2019L0572).

References

[1] Lorenz E N 1963 *J. Atmos. Sci.* **20** 130
[2] Chen G and Ueta T 1999 *Int. J. Bifurcat. Chaos* **9** 1465
[3] Lü J and Chen G 2002 *Int. J. Bifurcat. Chaos* **12** 659
[4] Čelikovský S and Chen G 2002 *Int. J. Bifurcat. Chaos* **12** 1789
[5] Čelikovský S and Chen G 2005 *Chaos Soliton. Fract.* **26** 1271
[6] Zhang D, Shi J Q, Sun Y, Yang X H and Ye Lei 2019 *Acta Phys. Sin.* **68** 240502 (in Chinese)
[7] Yang Q, Chen G and Huang K 2007 *Int. J. Bifurcat. Chaos* **17** 3929
[8] Le X, Zhang S and Zeng Y 2018 *Chin. J. Phys.* **56** 2381
[9] Dadras S, Momeni H R and Qi G 2010 *Nonlinear Dyn.* **62** 391
[10] Zolfaghari-Nejad M, Charmi M and Hassanpoor H 2022 *Complexity* **2022** 4488971
[11] Mobayen S, Volos C K, Kaar S and Avuolu N 2018 *Nonlinear Dyn.* **91** 939
[12] Ding P F, Feng X Y and Wu C M 2020 *Chin. Phys. B* **29** 108202
[13] Qi G, Chen G, Du S, Chen Z and Yuan Z 2005 *Physica A* **352** 295
[14] Vaidyanathan S 2012 *Adaptive controller and synchronizer design for the Qi-Chen chaotic system* (Berlin: Springer Berlin Heidelberg)
[15] Luo R 2008 *Phys. Lett. A* **372** 648
[16] Song L, Yang J and Xu S 2010 *Nonlinear Anal.* **72** 2326
[17] Li J F, Li N, Liu Y P and Gan Y 2008 *Acta Phys. Sin.* **58** 779 (in Chinese)
[18] Qi G and Zhang J 2017 *Chaos Soliton. Fract.* **99** 7
[19] Wu W, Chen Z and Yuan Z 2009 *Chaos Soliton. Fract.* **41** 2756
[20] Harrington H A and Gorder R A V 2017 *Nonlinear Dyn.* **88** 715
[21] Esen O, Choudhury A G and Guha P 2016 *Int. J. Bifurcat. Chaos* **26** 1650215
[22] Wang J, Chen Z, Che G and Yuan Z 2008 *Int. J. Bifurcat. Chaos* **18** 3309
[23] Wang J Z, Chen Z Q and Yuan Z Z 2006 *Chin. Phys.* **15** 1216
[24] Jia H Y, Chen Z Q and Yuan Z Z 2009 *Acta Phys. Sin.* **58** 4469 (in Chinese)
[25] Chen Z, Yang Y, Qi G and Yuan Z 2007 *Phys. Lett. A* **360** 696
[26] Wu W and Chen Z 2010 *Nonlinear Dyn.* **60** 615
[27] Artuso R, Aurell E and Cvitanovic P 1990 *Nonlinearity* **3** 325
[28] Artuso R, Aurell E and Cvitanovic P 1990 *Nonlinearity* **3** 361
[29] Lan Y and Cvitanović P 2004 *Phys. Rev. E* **69** 16217
[30] Dong C 2022 *Fractal and Fractional* **6** 190
[31] Lan Y and Li Y C 2008 *Nonlinearity* **21** 2801
[32] Wang D, Wang P and Lan Y 2018 *Phys. Rev. E* **98** 042204
[33] Azimi S, Ashtari O and Schneider T M 2022 *Phys. Rev. E* **105** 014217
[34] Boghosian B M, Brown A, Lätt J, Tang H, Fazendeiro L M and Coveney P V 2011 *Philos. Trans. Roy. Soc. A* **369** 2345
[35] Hao B L and Zheng W M 1998 *Applied Symbolic Dynamics and Chaos* (Singapore: World Scientific) pp. 6–10
[36] Cvitanović P, Artuso R, Mainieri R, Tanner G and Vattay G 2012 *Chaos: Classical and Quantum* (Copenhagen: Niels Bohr Institute)
[37] Press W H, Teukolsky S A, Veterling W T and Flannery B P 1992 *Numerical Recipes in C* (Cambridge: Cambridge University Press)
[38] Galias Z and Tucker W 2011 *Int. J. Bifurcat. Chaos* **21** 551
[39] Strogatz S H 2000 *Nonlinear Dynamics and Chaos: With Applications to Physics, Biology, Chemistry, and Engineering* (Cambridge: Perseus Books Publishing) pp. 312–313
[40] Wiggins S, Wiggins S and Golubitsky M 2003 *Introduction to applied nonlinear dynamical systems and chaos* (New York: Springer)
[41] Guckenheimer J and Holms P 1983 *Nonlinear Oscillations, Dynamical Systems, and Bifurcation of Vector* (New York: Springer)